ISSN 0038-0946, Solar System Research, 2021, Vol. 55, No. 1, pp. 47–60. © Pleiades Publishing, Inc., 2021.
Russian Text © The Author(s), 2021, published in Astronomicheskii Vestnik, 2021, Vol. 55, No. 1, pp. 50–64.

Rotational Dynamics of the Inner Satellites of Jupiter

V. V. Pashkevich[a], *, A. N. Vershkov[a], and A. V. Mel'nikov[a]

[a]*Central Astronomical Observatory at Pulkovo of RAS, St. Petersburg, Russia*

**e-mail: apeks@gaoran.ru*

Received March 3, 2020; revised September 4, 2020; accepted September 8, 2020

Abstract—The article considers the attitude stability of synchronous rotation and the most significant relativistic effects in the rotational dynamics of the inner satellites of Jupiter: Metis (J16), Adrastea (J15), Amalthea (J5), and Thebe (J14). It is established that the plane synchronous rotation of all inner satellites of Jupiter for the most probable values of the parameters of their shapes is stable with respect to tilting the axis of rotation. For the first time, the most significant secular, periodic, and mixed terms of the geodetic rotation of the inner satellites of Jupiter in the Euler angles relative to their own coordinate systems and in the angles of their rotation with respect to the fixed equator of the Earth and the vernal equinox (for the J2000.0 epoch) are determined. It is shown that there are objects in the Solar System with significant geodetic rotation caused primarily by their proximity to the perturbing central body rather than its mass. In particular, the value of the geodetic precession of the inner satellites of Jupiter (for which Jupiter is a less massive perturbing central body than the Sun) is 10^5 times greater than that of Jupiter rotating around its more massive central body (the Sun) and comparable with their precession in Newton approximation.

Keywords: satellites of Jupiter, Amalthea, Thebe, Adrastea, Metis, rotational dynamics, relativistic rotation, geodetic precession, geodetic nutation

DOI: 10.1134/S0038094620330035

INTRODUCTION

The inner satellites of Jupiter (Amalthea group) include Amalthea (J5), Thebe (J14), Adrastea (J15), and Metis (J16). The first of this group of satellites, Amalthea, was discovered in 1892 by E. Barnard by visual observation. In 1979, the first detailed images of Amalthea were obtained using the interplanetary spacecraft *Voyager-1.* The images showed (Smith et al., 1979a) that it has a very elongated (irregular) shape and is in the synchronous rotation mode. Three other small inner satellites of Jupiter were discovered in the same year from the analysis of images obtained by the *Voyager-2* spacecraft (Smith et al., 1979b). Later, Thomas et al. (1998) determined the shape, color, and reflecting properties of the surfaces of these satellites based on the images of Metis, Amalthea, and Thebe obtained in 1997 by the *Galileo* spacecraft and found that all the satellites are in the synchronous rotation mode. In the case of Adrastea, only estimates of its size were obtained (mean radius of the object is $R \approx 8.2$ km). Observations of Metis and Adrastea made by the *Cassini* spacecraft in 2000–2001 made it possible to specify parameters of their orbits (Porco et al., 2003).

Theoretical studies show (see, e.g., (Peale, 1977, 1999; Goldreich and Peale, 1966)) that the most probable final mode of the long-term tidal evolution of the satellite rotational motion is its rotation synchronous with the orbital motion. In this final mode, the rotation axis of the satellite coincides with the smallest axis of the figure of the satellite (the axis of the largest moment of inertia) and is orthogonal to the orbit plane, being the so-called plane rotation of the satellite. In the case of the plane rotation of the satellite in the exact synchronous spin-orbital resonance, the longest axis of the figure of the satellite in the pericenter of its orbit is parallel to the radius-vector "satellite mass center–planet," and when moving in orbit, it is oriented toward the planet and experiences librations (particularly due to the eccentricity of the orbit, see, e.g., (Beletskii, 1965)).

The vast majority of satellites of the planets of the Solar System, for which the rotation mode was found from the analysis of observations, are in synchronous rotation. Amalthea's synchronous rotation mode was established by Smith et al. (1979a) from the analysis of data from the *Voyager-1* spacecraft. It was also noted that the longest axis of the Amalthea's figure during its orbital motion is oriented toward Jupiter. Thomas et al. (1998) analyzed the images obtained by the *Galileo* spacecraft and found that Metis, Amalthea, and Thebe were in the plane synchronous rotation mode. The longest axis of the figure of each of the listed satellites (figures of the satellites were approximated by three-axis ellipsoids with homogeneous density) is

directed to Jupiter, and its orientation experiences librations with an amplitude not exceeding 5 degrees of arc. The low resolution of images obtained by *Galileo* made it impossible to draw any conclusion about Adrastea's rotation mode. However, Thomas et al. (1998) believed that Adrastea is captured in a synchronous spin-orbital resonance. This is indicated by the theoretical assessment of the timescale for tidal despinning of the initially rapid satellite rotation to the synchronous rotation (see (Peale, 1977, 1999)). According to Peale (1999), timescale for tidal despinning for the inner satellites of Jupiter are several thousand years, i.e., all satellites completed their tidal rotational evolution and should be captured in the synchronous resonance, if the rotation in it is stable. Study of the stability of the plane synchronous rotation of the inner satellites of Jupiter is important because of the fact that there are various perturbing factors in the rotational dynamics of these satellites. For example, the presence of large craters on the surfaces of Amalthea and Thebe (Thomas et al., 1998) indicates that the satellites collided with massive objects. The collision, in addition to affecting the shape of the satellite, can lead to changes in its orientation in space and rotational speed; a satellite in an unstable plane synchronous rotation can be captured in another spin-orbiting resonance or go into the chaotic rotation mode (Wisdom, 1987).

Since Jupiter is the second largest object by mass in the Solar System, we should expect that it will cause relativistic perturbations in the dynamics of bodies close to it. The most significant relativistic effects in the rotation of celestial bodies are the effects of geodetic precession and nutation, together constituting the geodetic rotation. The effect of geodetic precession, first considered in 1916 by de Sitter (1916), is a systematic change in the direction of the axis of rotation of the celestial body as a result of the parallel transfer of the angular momentum vector of the body along its orbit in curved space-time. The effect of geodetic nutation introduced in 1991 by Fukushima (1991) is a periodic change in the direction of the celestial body's rotation axis, which occurs for the same reason as the geodetic precession.

The systematic or secular change can be represented as a polynomial in the degree of time:

$$\Delta x_I = \sum_{n=0}^{N} \Delta x_n t^n,$$

where t is the time, Δx_n are coefficients of the secular terms, and N is the degree of the approximating polynomial.

In celestial mechanics, the nutation motion of the body's axis of rotation is traditionally called periodic, although it can be described by both periodic Fourier series or, in addition, by mixed Poisson time series (see, e.g., (Woolard, 1963; Abalakin, 1979; Brumberg and Bretagnon, 2000)). This article is no exception. In it, the effect of geodetic nutation is presented as a sum of periodic Fourier terms and mixed Poisson time series (which will be referred to in the article as *periodic* and *mixed* terms):

$$\Delta x_{\text{II}} = \sum_j \sum_{k=0}^{M} (\Delta x_{Cjk} \cos(\nu_{j0} + \nu_{j1} t) + \Delta x_{Sjk} \sin(\nu_{j0} + \nu_{j1} t)) t^k,$$

where t is the time; the summation index j determines the number of summed terms; Δx_{Sjk}, Δx_{Cjk} are the coefficients of periodic terms and time-mixed Poisson terms; ν_{j0}, ν_{j1} are the phases and frequencies of the body under study; and M is the approximation parameter.

Note that in this article, where it is not specifically mentioned, the term *value of geodetic precession* means the value of its rate.

Theoretical estimates of the value of the geodetic precession of two Jovian satellites, Io (J1) and Metis (J16), were obtained in Biscani and Carloni (2015). A simplified model of satellite rotation was considered, namely it was assumed that the satellites are homogeneous spheres, and the reference planes were chosen perpendicular to the axis of rotation of the planet. Mel'nikov et al. (2019) considered the rotation dynamics of a number of small satellites of the planets of the Solar System, with established rotation parameters. In particular, it was found that the value of the geodetic precession of one of the nearest Jovian satellites, Amalthea, was 50 times higher than the value of the geodetic precession of Mercury. According to (Pashkevich, 2016), Mercury has the largest geodetic precession among the planets of the Solar System because it is the nearest planet to the Sun (the most massive body of the Solar System). Therefore, the relativistic effects in the rotation of the nearest Jupiter's satellites of the Amalthea group should be studied in more detail.

The objectives of this study were to investigate the character of the attitude stability of synchronous rotation and determine the most significant secular and periodic terms of the geodetic rotation of the inner satellites of Jupiter: Metis, Adrastea, Amalthea, and Thebe (satellites are listed in ascending order of distance from Jupiter). The methods developed by Mel'nikov and Shevchenko (2000, 2007) were used to study the rotation stability of the satellites. Secular and periodic terms of the geodetic rotation of satellites were calculated using the method for studying the geodetic rotation of any bodies of the Solar System (Pashkevich, 2016) with long-time ephemerides.

Table 1. Orbital and physical parameters of the inner satellites of Jupiter: Data from (Thomas et al., 1998; Burns et al., 2003; Porco et al., 2003)

	Metis (J16)	Adrastea (J15)	Amalthea (J5)	Thebe (J14)
a_s, km	128000	129000	181400	221900
e	0.0002	0.0015	0.0031	0.0177
$a \times b \times c$, km	30 × 20 × 17	10 × 8 × 7	125 × 73 × 64	58 × 49 × 42
ω_0	1.0742	0.8115	1.2141	0.7079

ATTITUDE STABILITY OF PLANE SYNCHRONOUS ROTATION

The dynamics of the plane (in the plane of orbit) rotational motion of the satellite in the gravitational field of the planet can be described within the model of the perturbed mathematical pendulum. Next, we assume that the axis of rotation of the satellite coincides with the smallest axis of the figure of the satellite and is orthogonal to the plane of orbit. Let us define the angle φ as the angle between the apsidal line and the longest axis of the figure of the satellite, then the angle $\varphi - f$, where f is the true anomaly, will represent the angle between the longest axis of the figure of the satellite and the direction to the planet. The equation of plane translational–rotational motion of the satellite is as follows (Goldreich and Peale, 1966; Wisdom, 1987):

$$\frac{d^2\varphi}{dt^2} + \frac{\omega_0^2}{2r^3}\sin 2(\varphi - f) = 0, \qquad (1)$$

where the parameter $\omega_0 = \sqrt{3(a^2 - b^2)/(a^2 + b^2)}$ characterizes the asymmetry of the figure of the satellite, $a > b > c$ are the main axes of inertia of the triaxial ellipsoid with homogeneous density which approximates the figure of the satellite; $r = a_s(1 - e^2)/(1 + e\cos f)$ is the "planet–satellite" distance, e is the eccentricity of the orbit of the satellite, and a_s is the semimajor axis of the orbit. According to (1), the dynamics of the plane rotational motion of the satellite are determined by the value of the eccentricity of the orbit e and the value of the parameter ω_0. Then, we assume $a_s = 1$ and $GM = 1$, where G is the universal gravitational constant, and M is the mass of the planet. Therefore, one orbital period of the satellite corresponds to 2π units of time.

At certain values of e and ω_0, the equation of the planar rotational motion of the satellite has two stable odd 2π-periodic solutions (Torzhevskii et al., 1964), i.e., there are two modes of synchronous resonance in the phase space of the plane rotational motion of the satellite. One corresponds to a synchronous α-resonance and the other to a synchronous β-resonance. The above terminology was used in (Mel'nikov and Shevchenko, 2000, 2007).

Mel'nikov and Shevchenko (2000, 2007) studied the rotational dynamics of small satellites of the planets of the Solar System and found that several modes of synchronous resonance exist simultaneously in the phase space of the plane rotational motion of a number of satellites, in particular, in the case of Amalthea. In the course of the tidal evolution of rotational motion, Amalthea can be captured in one of the synchronous resonance modes if the plane rotation in it is Lyapunov stable with respect to tilting the axis of rotation of the satellite to the plane of orbit. If the plane synchronous rotation of the satellite is unstable, the satellite can go into chaotic "tumbling" mode (Wisdom, 1987) in the presence of perturbations (e.g., a *collision/close rapprochement* with other bodies) leading to a shift in the rotation axis from normal. The study of the stability of the Amalthea rotational dynamics showed (Mel'nikov and Shevchenko, 2000) that the synchronous α-resonance is unstable and the synchronous β-resonance is stable, i.e., Amalthea is currently captured in the synchronous β-resonance. This is confirmed by the small ($<5°$) amplitude of the observed librations (Thomas et al., 1998) of the orientation of the longest axis of the Amalthea figure with respect to the direction to Jupiter during its orbital motion. If Amalthea were in the synchronous α-resonance, the amplitude of the librations could reach 30°.

In the cases of Metis and Thebe, the amplitudes of observed librations (Thomas et al., 1998) are also small, and their periods coincide with the periods of the satellite orbital motion. Low resolution of *Galileo* satellite images made it impossible to detect librations of the figure orientation for Adrastea. It should be noted that determination of the amplitude of librations by analyzing observational data obtained from interplanetary spacecraft makes it possible to specify dynamic parameters of satellites, in particular the values of moments of inertia (see, e.g., Tiscareno et al., 2009).

Next, let us consider the attitude stability of the plane synchronous rotation for Metis, Adrastea, and Thebe. We use methods and algorithms developed by Mel'nikov and Shevchenko (2000, 2007) to study the attitude stability of the plane rotation of satellites.

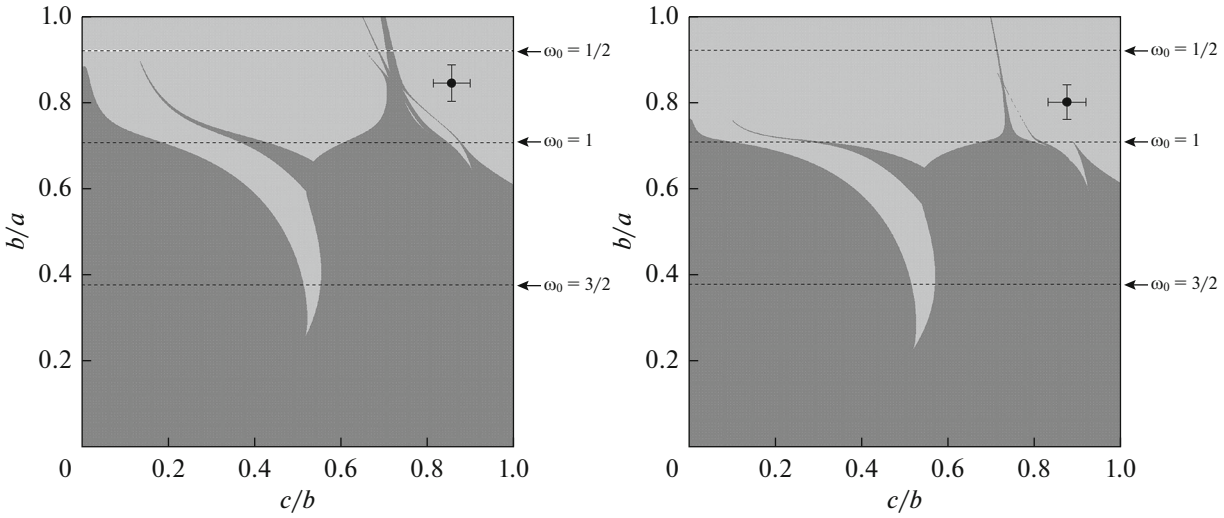

Fig. 1. Regions of stability (light) and instability (dark) relative to the slope of the satellite's axis of rotation in the center of the synchronous α-resonance: the left panel, $e = 0.0015$, $\omega_0 = 0.8115$ (Adrastea) and, the right panel, $-e = 0.0177$, $\omega_0 = 0.71079$ (Thebe). Satellite positions are indicated by points with error bars. Dashed horizontal lines correspond to the values of ω_0 given on the right.

Table 1 shows the values of orbital and physical parameters of the inner satellites of Jupiter used in stability analysis. According to (Mel'nikov and Shevchenko, 2007), for the parameter values presented in Table 1, in the cases of Adrastea and Thebe, there is only a synchronous α-resonance, and in the case of Metis and Amalthea, there is a synchronous α-resonance and a synchronous β-resonance.

The stability analysis of the Lyapunov plane synchronous rotation for Metis, Adrastea, and Thebe was carried out using numerical integration of differential equations describing the spatial rotation of the satellite (see (Mel'nikov and Shevchenko, 2000, 2007)) and the computation of the Lyapunov characteristic exponent (LCE) for a set of all possible values of the parameters of the satellite figures (c/b, b/a) and the fixed value of e.

LCEs represent the average rate of exponential divergence of close (in terms of initial conditions) phase space trajectories of a dynamic system (for more details about LCE, see, e.g., (Lichtenberg and Lieberman, 1984)). The Hamiltonian system with N degrees of freedom has $2N$ Lyapunov exponents: $L_i \geq L_{i+1}$, $i = 1, ..., 2N-1$, which form symmetrical pairs: $L_j = -L_{j+N}$, $j = 1, ..., N$. The nonzero value of the maximum LCE, L_1, indicates chaotic (unstable) motion and zero indicates regular (stable) motion.

LCEs were calculated for phase space trajectories corresponding to the satellite rotation in exact synchronous resonance. First, coordinates of the synchronous resonance center were determined (separately for α-resonance and β-resonance) in the plane problem of the set of values of the parameter b/a (0, 1] for the selected value of e at the phase space section $(\varphi, d\varphi/dt)$ determined in the satellite orbit pericenter (see examples of phase space section for different satellites in (Wisdom, 1987; Shevchenko, 1999; Mel'nikov and Shevchenko, 2000, 2007, 2008)). In the case of the plane rotation of a satellite with homogeneous density, these coordinates are determined only as $\omega_0 = \sqrt{3(1-(b/a)^2)/(1+b/a)^2)}$ and e. Then, LCEs were calculated for different values of $c/b \in (0, 1]$ and $b/a \in (0, 1]$ on a high-resolution grid. The step of the grid on the plane $(c/b, b/a)$, in the nodes of which the LCE was calculated, was set to 0.001 on both axes. The entire LCE spectrum (in our case, $N = 3$, i.e., there are six LCEs) was calculated at the integration time interval of 10^6 orbital periods using the algorithm presented in (Kouprianov and Shevchenko, 2003). The boundaries of stable (the maximal LCE is zero) and unstable dynamics (the maximal LCE is greater than zero) of the satellite rotational motion in the exact synchronous resonance were determined on the basis of the analysis of calculated values of maximal LCE (L_1) on planes $(c/b, b/a)$.

The stability diagrams constructed in this way for all satellites are presented in Figs. 1 and 2. The analysis of stability diagrams of Adrastea and Thebe showed that the rotation of both satellites in the only possible synchronous α-resonance is stable for the most probable parameters of their figures. The stability diagrams (see Fig. 1) show that Adrastea and Thebe are far from the regions with unstable dynamics. According to Fig. 2, for the most probable parameters of the figure of Metis, its rotation in the synchronous α-resonance is unstable (on the stability diagram, Metis is in the

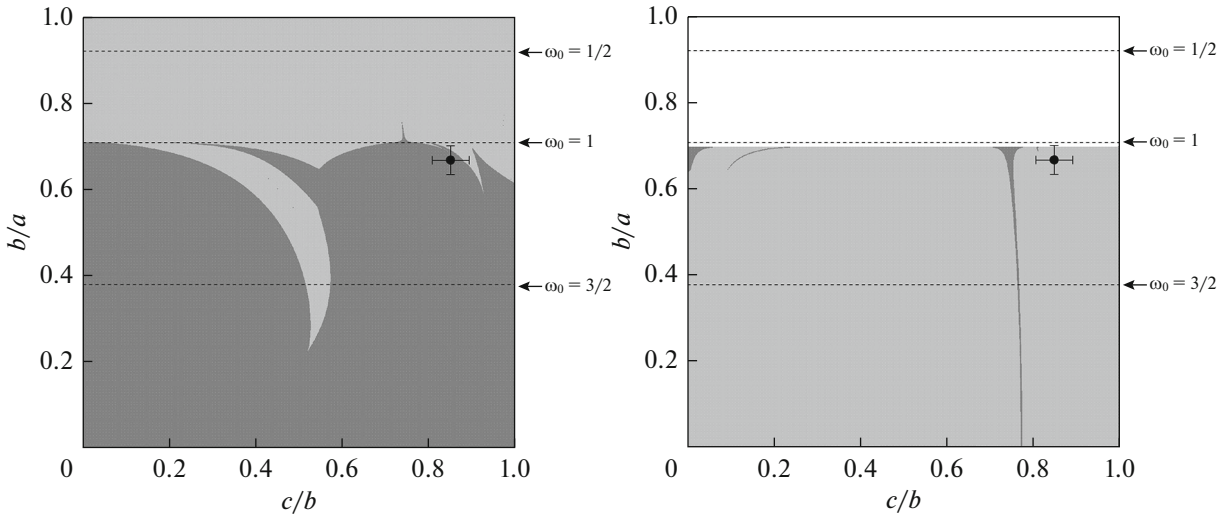

Fig. 2. Regions of stability (light) and instability (dark) relative to the slope of the satellite's axis of rotation in the center of the synchronous α-resonance (left) and synchronous β-resonance (right), $e = 0.0002$, $\omega_0 = 1.1717$ (Metis). There is no synchronous β-resonance in the white region. The position of Metis (J16) is indicated by the point with the error bars. Dashed horizontal lines correspond to the values of ω_0 given on the right.

region with unstable dynamics) and in the synchronous β-resonance, it is stable.

Therefore, we established that the plane synchronous rotation of all inner satellites of Jupiter is stable with respect to tilting of the rotation axis to the plane of orbit. Perturbations in the rotational dynamics of the considered satellites, such as collision/close rapprochement with other bodies and the subsequent insignificant modification of the satellite shape (ω_0 values) or the value and direction of its angular velocity vector, will not cause the satellite to leave the plane synchronous rotation mode. Next, consider the relativistic effects in the rotational dynamics of the inner satellites of Jupiter.

RELATIVISTIC EFFECTS IN SATELLITE ROTATION

The effects of geodetic rotation of the inner satellites of Jupiter were studied with respect to the kinematically nonrotating coordinate system of the studied bodies (Kopeikin et al., 2011; Archinal et al., 2018). The positions, velocities, and orbital elements of the satellites were taken from the Horizons On-Line Ephemeris System (Giorgini et al., 2001) at all time intervals of the ephemerides existence. Table 2 provides information on the research step and research time interval. For the Sun, large planets, the Moon and Pluto, the positions and velocities were calculated using the fundamental ephemeris JPL DE431/LE431 (Folkner et al., 2014).

Geodetic rotation rates of the inner satellites of Jupiter were calculated:

(a) In the rotation angles of the satellites (α_0, δ_0, W) with respect to the Earth's fixed equator of the J2000.0 epoch defined in the International Celestial Reference Frame (ICRF) (Ma et al., 1998), and the points of the vernal equinox of the J2000.0 epoch.

(b) In the Euler angles (ψ, θ, φ) with respect to the coordinate systems of these satellites (Archinal et al., 2018), the origin of which coincides with their mass centers.

The angular velocity vector of the geodetic rotation for any bodies of the Solar System is determined by the following formula (Eroshkin and Pashkevich, 2007; Pashkevich and Eroshkin, 2018):

Table 2. Time Interval and Step of Research

Satellite	Research time interval	Step
Metis	400 years (from Dec. 19 AD1799 to Jan. 13, AD2200)	42 min
Adrastea	400 years (from Dec. 19, AD1799, to Jan. 13, AD2200)	42 min
Amalthea	1000 years (from Feb. 7, AD1600, to Dec. 6, AD2599)	60 min
Thebe	400 years (from Dec. 19, AD1799, to Jan. 13, AD2200)	90 min

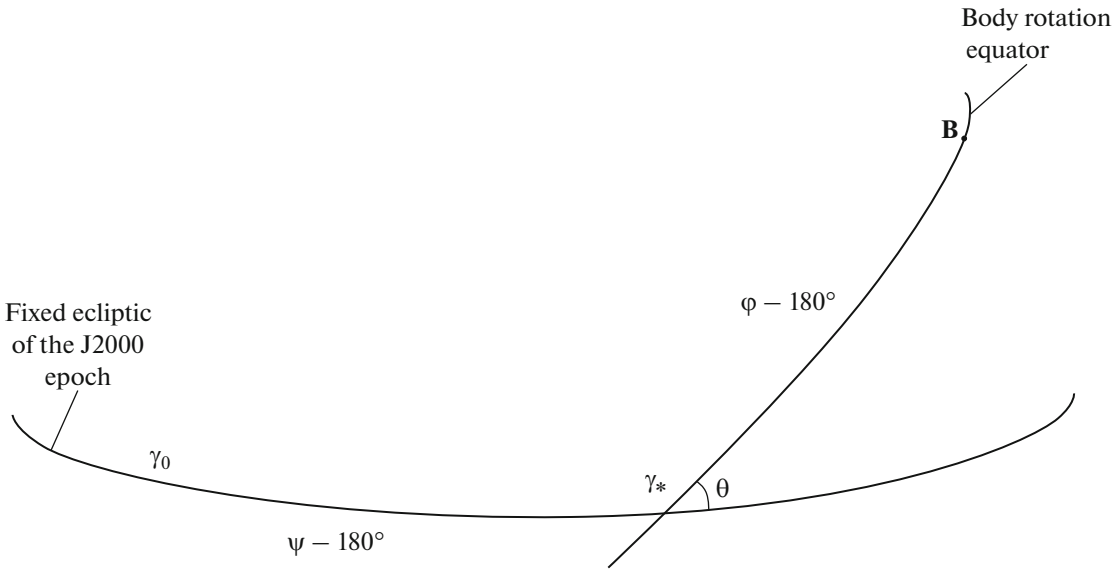

Fig. 3. Euler angles (ψ, θ, φ) that define the rotation of the Solar System bodies.

$$\bar{\sigma}_i = \frac{1}{c^2}\sum_{j\neq i}\frac{Gm_j}{\left|\bar{R}_i - \bar{R}_j\right|^3}\left(\bar{R}_i - \bar{R}_j\right)\times\left(\frac{3}{2}\dot{\bar{R}}_i - 2\dot{\bar{R}}_j\right). \quad (2)$$

Here, c is the speed of light in a vacuum; G is the gravitational constant; the index i corresponds to the studied bodies (inner satellites of Jupiter) and j corresponds to the perturbing bodies; $\bar{R}_i, \dot{\bar{R}}_i, \bar{R}_j, \dot{\bar{R}}_j$ are the barycentric vectors of positions and velocities of the ith and jth bodies, respectively; m_j is the mass of the jth body; and the symbol × indicates the vector product. Next, the index i is omitted in formulas. As it can be seen from formula (2), the value of the vector of the geodetic rotation of the satellite is $|\bar{\sigma}| \sim \frac{M}{r^{2.5}}$, where $m_{j=M} = M$ is the mass of the central body (Jupiter), and $\left|\bar{R}_i - \bar{R}_{j=M}\right| = r$ is the distance to it, i.e., it significantly depends on the proximity of the satellite to the central body. In particular, it follows from formula (2) that the geodetic rotation of the body depends only on the masses of the perturbing bodies and the distance to them and does not depend on the mass of the body itself.

The rates of geodetic rotation of the inner satellites of Jupiter are determined in Euler angles as follows (Pashkevich and Vershkov, 2019):

$$\left.\begin{aligned}\Delta\dot{\psi} &= -\frac{\sigma_1\sin\varphi + \sigma_2\cos\varphi}{\sin\theta}\\ \Delta\dot{\theta} &= -\sigma_1\cos\varphi + \sigma_2\sin\varphi\\ \Delta\dot{\varphi} &= \sigma_3 - \Delta\dot{\psi}\cos\theta\end{aligned}\right\}. \quad (3)$$

Here, ψ is the longitude angle of the descending node of the equator of the body on the J2000.0 epoch ecliptic; θ is the inclination angle of the body equator to the fixed J2000.0 epoch ecliptic; φ is the body's proper rotation angle between the descending node of the J2000.0 epoch and the principal axis of the minimum moment of inertia of the body passing through the point **B** at the equator of the body rotation (Fig. 3); $\Delta\dot{\psi} = \dot{\psi}_r - \dot{\psi}$, $\Delta\dot{\theta} = \dot{\theta}_r - \dot{\theta}$, and $\Delta\dot{\varphi} = \dot{\varphi}_r - \dot{\varphi}$ are the differences between the relativistic and Newtonian velocities of Euler angles of the investigated body, respectively; the dot indicates time differentiation; and σ_1, σ_2, σ_3 are reduced (Pashkevich, 2016) components of angular velocity vector (2) of the geodetic rotation of the inner satellites of Jupiter from the geocentric coordinate system (coordinate system of ephemeris DE431/LE431) to the planetocentric coordinate system (Archinal et al., 2018).

The configuration of the angles of rotation of the bodies of the Solar System (α_0, δ_0, W) presented in Fig. 4 is similar to the configuration for the Euler angles (Fig. 3). Here, α_0 is the right ascension of the body's north pole of rotation; δ_0 is the declination of the body's north pole of rotation; W = QB is the angular distance of the body's zero meridian measured by the body's equator from the fixed Earth equator of the J2000.0 epoch. The expressions for the rates of geodetic rotation of the inner satellites of Jupiter in angles of their rotation are obtained by replacing the Euler angles with the corresponding angles of rotation of satellites ($\psi \to 270° + \alpha_0$, $\theta \to 90° - \delta_0$, $\varphi \to 180° + W$) from expressions (3):

$$\left.\begin{aligned}\Delta\dot{\alpha}_0 &= \frac{\sigma_1\sin W + \sigma_2\cos W}{\cos\delta_0}\\ \Delta\dot{\delta}_0 &= -\sigma_1\cos W + \sigma_2\sin W\\ \Delta\dot{W} &= \sigma_3 - \Delta\dot{\alpha}\sin\delta_0\end{aligned}\right\}, \quad (4)$$

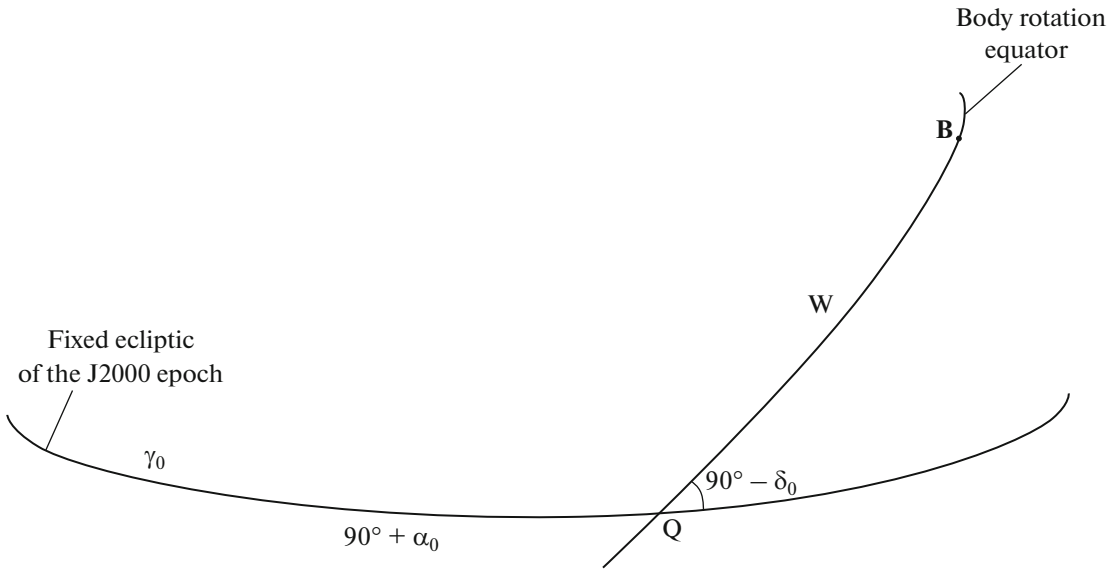

Fig. 4. Rotational angles of the Solar System bodies (α_0, δ_0, W).

where $\Delta\dot{\alpha}_0 = \dot{\alpha}_{0r} - \dot{\alpha}_0$, $\Delta\dot{\delta}_0 = \dot{\delta}_{0r} - \dot{\delta}_0$, and $\Delta\dot{W} = \dot{W}_r - \dot{W}$ are the differences in relativistic and Newtonian rotational speeds of the body under study, respectively; the dot indicates time differentiation.

The most significant components of the geodetic rotation rate of the body under study were determined using the methods of least squares and spectral analysis (Pashkevich, 2016). As a result, the values of coefficients of basic secular, periodic, and mixed terms of the geodetic rotation rate of the body are calculated. Expressions describing the speed of geodetic rotation of the body are presented in the following form:

$$\Delta\dot{x} = \Delta\dot{x}_{\rm I} + \Delta\dot{x}_{\rm II} = \sum_{n=1}^{N}\Delta\dot{x}_n t^{n-1} + \sum_{j}\sum_{k=0}^{M}(\Delta\dot{x}_{Cjk}\cos(\nu_{j0} + \nu_{j1}t) + \Delta\dot{x}_{Sjk}\sin(\nu_{j0} + \nu_{j1}t))t^k, \quad (5)$$

where $\Delta\dot{x}_n$ are the coefficients of secular terms; $\Delta\dot{x}_{Sjk}$, $\Delta\dot{x}_{Cjk}$ are the coefficients of periodic terms and mixed terms; $\dot{x} = \dot{\psi}, \dot{\theta}, \dot{\varphi}, \dot{\alpha}_0, \dot{\delta}_0, \dot{W}$; ν_{j0}, ν_{j1} are the phases and frequencies of the investigated body, which are the combinations of the corresponding Delaunay arguments and mean longitudes of the perturbing bodies; the summation index j determines the number of summed periodic terms and its value changes for each investigated body; t is the time in Julian days; and N and M are the approximation parameters.

Figure 5 shows the calculated rate of the geodetic rotation of the inner satellites of Jupiter in Euler angles. The white line in the diagrams shows a secular variation.

After the analytical integration of expression (5), secular, periodic, and mixed terms of the geodetic rotation of the body are calculated:

$$\Delta x = \Delta x_{\rm I} + \Delta x_{\rm II} = \sum_{n=1}^{N}\Delta x_n t^n + \sum_{j}\sum_{k=0}^{M}(\Delta x_{Cjk}\cos(\nu_{j0} + \nu_{j1}t) + \Delta x_{Sjk}\sin(\nu_{j0} + \nu_{j1}t))t^k, \quad (6)$$

where $\Delta x_n = \dfrac{\Delta\dot{x}_n}{n}$, $x = \psi, \theta, \varphi, \alpha_0, \delta_0, W$, and the coefficients of sine and cosine are calculated as follows:

$$\Delta x_{SjM} = \frac{\Delta\dot{x}_{CjM}}{\nu_{j1}}, \quad \Delta x_{CjM} = \frac{-\Delta\dot{x}_{SjM}}{\nu_{j1}},$$
$$\Delta x_{SjM-1} = \frac{\Delta\dot{x}_{CjM-1} - m\Delta x_{CjM}}{\nu_{j1}},$$
$$\Delta x_{CjM-1} = \frac{m\Delta x_{SjM} - \Delta\dot{x}_{SjM-1}}{\nu_{j1}}, \quad (7)$$
$$\ldots$$
$$\Delta x_{Sj1} = \frac{\Delta\dot{x}_{Cj1} - 2\Delta x_{Cj2}}{\nu_{j1}}, \quad \Delta x_{Cj1} = \frac{2\Delta x_{Sj2} - \Delta\dot{x}_{Sj1}}{\nu_{j1}},$$
$$\Delta x_{Sj0} = \frac{\Delta\dot{x}_{Cj0} - \Delta x_{Cj1}}{\nu_{j1}}, \quad \Delta x_{Cj0} = \frac{\Delta x_{Sj1} - \Delta\dot{x}_{Sj0}}{\nu_{j1}}.$$

The values of $N = 2$ and $M = 1$ were determined as a result of the studies using the least-squares method,

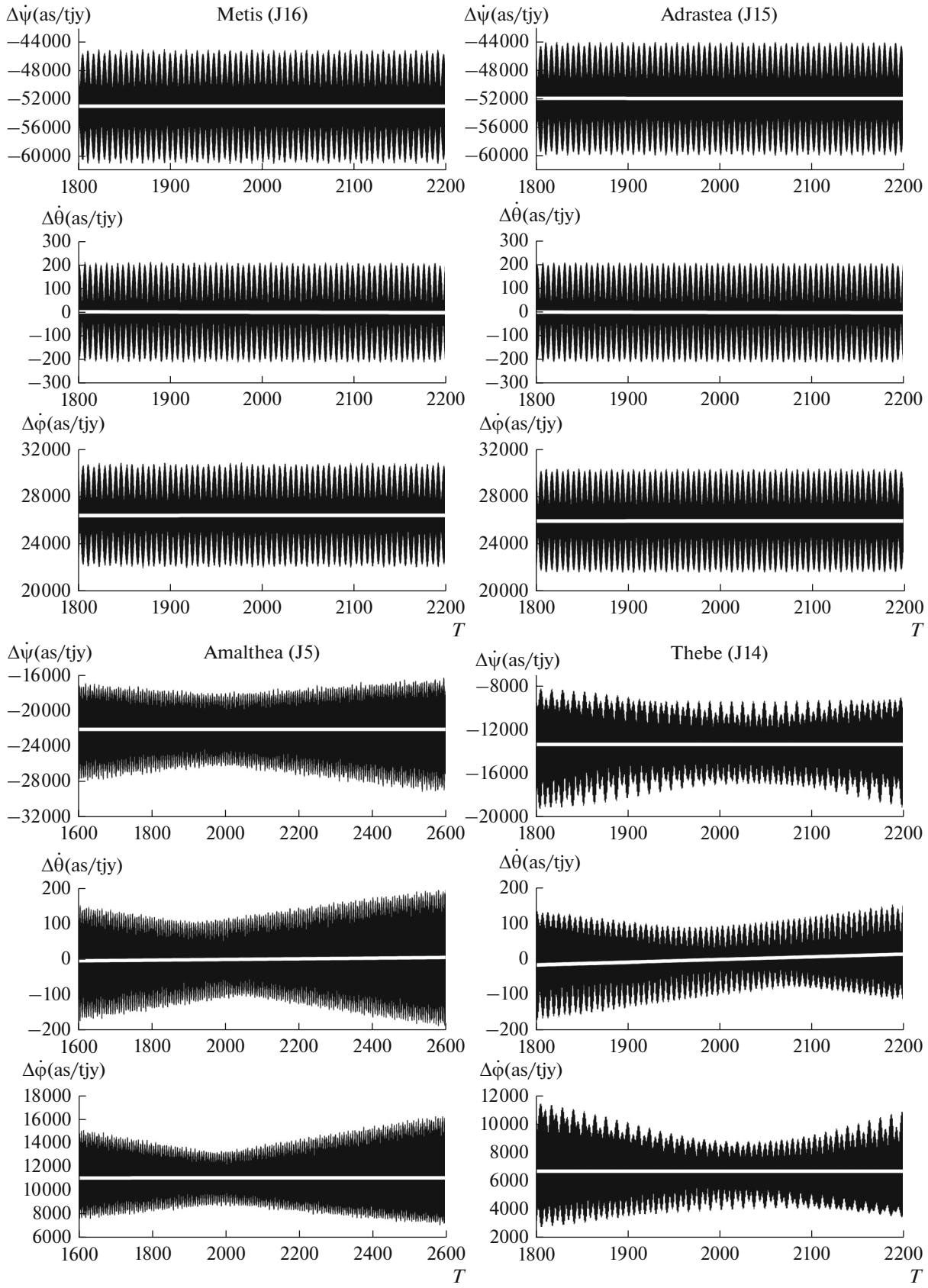

Fig. 5. Geodetic rotation rates of the inner satellites of Jupiter in Euler angles (T is the time in Julian years). The white line shows the secular variation.

Table 3. Secular terms of the geodetic rotation of Jupiter (Pashkevich and Vershkov, 2019) and its inner satellites calculated for Euler angles

	Metis (J16)	Adrastea (J15)	Amalthea (J5)	Thebe (J14)	Jupiter (J)
	$\Delta\psi_I$ (")	$\Delta\psi_I$ (")	$\Delta\psi_I$ (")	$\Delta\psi_I$ (")	$\Delta\psi_I$ (")
t	− 52957.2516	−51932.8456	−22118.2274	−13372.5500	−0.2130
t^2	− 20.0929	− 19.7509	−0.7460	−2.8287	0.0035
	$\Delta\theta_I$ (")	$\Delta\theta_I$ (")	$\Delta\theta_I$ (")	$\Delta\theta_I$ (")	$\Delta\theta_I$ (")
t	− 0.4232	− 0.4151	−0.0923	−2.4703	−0.0060
t^2	− 3.9838	− 3.9067	4.7351	37.7619	0.0001
	$\Delta\varphi_I$ (")	$\Delta\varphi_I$ (")	$\Delta\varphi_I$ (")	$\Delta\varphi_I$ (")	$\Delta\varphi_I$ (")
t	26460.9380	25949.0709	11055.1784	6693.8317	−0.0987
t^2	19.8858	19.5347	0.5755	2.8902	−0.0036

which provided the best approximation of geodetic rotation parameters.

Tables 3–5 show the calculated values of secular (Tables 3 and 5), periodic, and mixed (Tables 4 and 5) terms of the geodetic rotation of the inner satellites of Jupiter. In Tables 3 and 4: t is the Barycentric Dynamical Time (BDT) measured in thousands of Julian years (tjy) (365250 days) from the J2000 epoch.

As can be seen from Table 3, the calculated value of the linear term of the geodetic precession of Metis is $\Delta\psi_1 = -1°.4710348$ per century, which agrees well with the theoretical value of this magnitude, $-1°.473$ per century, obtained in (Biscani and Carloni, 2015) for a simplified model of the satellite rotation without a quadratic term. It should be noted that the presence of the quadratic term in Table 3 indicates a change in the value of the rate of geodetic rotation.

It should be noted that the value of the geodetic rotation of Jupiter (Pashkevich and Vershkov, 2019), which rotates around its more massive central body (the Sun), is 10^5 times smaller than that of the closest Jovian satellite (see Table 3), for which Jupiter is a less massive central body. From this, it follows that the Solar System has objects with high geodetic rotation rates due to their proximity to the perturbing central body, not its mass.

In Table 4, Ω_{L55}, Ω_{L514} are the longitudes of the ascending nodes (the orbits of the Jovian satellites) in the Laplace plane for Amalthea and Thebe, respectively; λ_5 is the mean longitude of Jupiter; λ_{55}, λ_{514}, λ_{515}, λ_{516} are the mean Jupiter-centric longitudes of Amalthea, Thebe, Adrastea, and Metis, respectively. The mean longitude of Jupiter was taken from (Brumberg and Bretagnon, 2000). The mean longitudes and longitudes of the ascending nodes of Jupiter's satellites are taken from (Archinal et al., 2018).

Table 5 presents the rotation angles (α_0, δ_0, W) of the inner satellites of Jupiter (Archinal et al., 2018) and the most significant secular, periodic, and mixed terms of their geodetic rotation calculated in this study ($\Delta\alpha_0$, $\Delta\delta_0$, ΔW). It should be noted that the time-mixed Poisson terms in formula (6) with the coefficients from Tables 4 and 5, which are used only in the model to describe the geodetic rotation, can only be used during research intervals (see Table 2). These terms describe very well long-period variations with incomplete periods presented in Fig. 5 as divergent amplitudes.

As can be seen from Tables 3 and 5, the values of the geodetic precession of the satellites increase as their distance from the central body, Jupiter, decreases, which makes a significant contribution to the values of right ascensions and declensions of the satellites considered (see Table 5). Therefore, e.g., for Metis (the closest satellite of Jupiter at the moment), the value of the geodetic precession in right ascension α_0 exceeds the resulting value of its right ascension $\Delta\alpha_0$ by 13 times in absolute value, and the value of the geodetic precession in declination $\Delta\delta_0$ exceeds the resulting value of its declination δ_0 by seven times in absolute value. For Thebe (the farthest satellite from the considered satellites of Jupiter), these values ($\Delta\alpha_0$, $\Delta\delta_0$) exceed its α_0 and δ_0 by three and two times in absolute value, respectively. From this circumstance it follows that the Solar System has objects with significant geodetic rotation. Therefore, the value of the geodetic precession of the inner satellites of Jupiter is

Table 4. Periodic and mixed terms of the geodetic rotation of the inner satellites of Jupiter calculated for Euler angles

Body name	Angle	Period	Argument	Coefficient at sin(Argument) ("$\times 10^{-6}$)	Coefficient at cos(Argument) ("$\times 10^{-6}$)
Metis (J16)	$\Delta\psi_{II}$	7.0752 h	$\lambda_{516} - \lambda_5$	$-491.02 + 66.84t$	$406.71 + 77.88t$
		7.0742 h	$\lambda_{516} + \lambda_5$	$36.97 + 70.96t$	$326.50 - 3.60t$
	$\Delta\theta_{II}$	7.0752 h	$\lambda_{516} - \lambda_5$	$-12.11 - 0.68t$	$-4.19 + 1.84t$
		7.0742 h	$\lambda_{516} + \lambda_5$	$12.68 - 0.25t$	$-1.43 - 2.68t$
	$\Delta\varphi_{II}$	7.0752 h	$\lambda_{516} - \lambda_5$	$191.16 - 11.21t$	$-46.80 - 30.55t$
		7.0742 h	$\lambda_{516} + \lambda_5$	$-36.99 - 70.18t$	$-326.96 + 3.90t$
Adrastea (J15)	$\Delta\psi_{II}$	7.1587 h	$\lambda_{515} - \lambda_5$	$-619.25 + 144.03t$	$-96.70 - 880.88t$
		7.1578 h	$\lambda_{515} + \lambda_5$	$-216.77 - 332.46t$	$240.02 - 294.02t$
	$\Delta\theta_{II}$	7.1587 h	$\lambda_{515} - \lambda_5$	$-4.80 + 16.84t$	$-11.64 - 7.06t$
		7.1578 h	$\lambda_{515} + \lambda_5$	$9.32 - 11.54t$	$8.41 + 12.88t$
	$\Delta\varphi_{II}$	7.1587 h	$\lambda_{515} - \lambda_5$	$159.02 - 163.79t$	$110.20 + 221.18t$
		7.1578 h	$\lambda_{515} + \lambda_5$	$217.02 + 333.29t$	$-240.32 + 295.24t$
Amalthea (J5)	$\Delta\psi_{II}$	143.7475 day	Ω_{L55}	$14788.07 - 20766.41t$	$-8065.69 - 240278.07t$
		71.8737 day	$2\Omega_{L55}$	$-705.83 + 8528.53t$	$1110.30 + 17772.11t$
		11.9577 h	$\lambda_{55} - \lambda_5$	$428.18 - 518.50t$	$221.47 + 672.87t$
		11.9549 h	$\lambda_{55} + \lambda_5$	$215.16 + 138.37t$	$-118.79 + 403.48t$
	$\Delta\theta_{II}$	143.7475 day	Ω_{L55}	$290.56 + 9211.87t$	$585.78 - 792.88t$
		71.8737 day	$2\Omega_{L55}$	$-16.61 - 340.18t$	$-27.57 + 162.20t$
		11.9577 h	$\lambda_{55} - \lambda_5$	$0.57 - 17.16t$	$9.58 - 2.20t$
		11.9549 h	$\lambda_{55} + \lambda_5$	$-4.61 + 15.81t$	$-8.33 - 5.39t$
	$\Delta\varphi_{II}$	143.7475 day	Ω_{L55}	$-14505.42 + 20809.18t$	$7964.79 + 240812.87t$
		71.8737 day	$2\Omega_{L55}$	$705.95 - 8528.58t$	$-1110.22 - 17772.10t$
		11.9577 h	$\lambda_{55} - \lambda_5$	$-90.20 + 232.96t$	$-118.14 - 114.91t$
		11.9549 h	$\lambda_{55} + \lambda_5$	$-215.48 - 138.61t$	$118.75 - 404.03t$
Thebe (J14)	$\Delta\psi_{II}$	291.3118 day	Ω_{L514}	$-20924.96 - 523207.02t$	$41738.74 - 1108462.06t$
		145.6559 day	$2\Omega_{L514}$	$871.19 + 180592.02t$	$-9582.70 + 175870.07t$
		16.1914 h	$\lambda_{514} - \lambda_5$	$-463.338 + 113.40t$	$137.40 + 384.96t$
		16.1863 h	$\lambda_{514} + \lambda_5$	$-76.85 + 288.85t$	$205.30 + 55.46t$
	$\Delta\theta_{II}$	291.3118 day	Ω_{L514}	$-1560.60 + 39956.22t$	$-871.89 - 19067.79t$
		145.6559 day	$2\Omega_{L514}$	$170.03 - 3080.78t$	$11.00 + 3191.90t$
		16.1914 h	$\lambda_{514} - \lambda_5$	$-7.24 - 3.94t$	$-6.81 + 4.93t$
		16.1863 h	$\lambda_{514} + \lambda_5$	$8.24 + 2.12t$	$2.76 - 9.20t$
	$\Delta\varphi_{II}$	291.3118 day	Ω_{L514}	$21951.15 + 524366.28t$	$-42198.58 + 1110937.40t$
		145.6559 day	$2\Omega_{L514}$	$-871.47 - 180591.77t$	$9582.78 - 175869.98t$
		16.1914 h	$\lambda_{514} - \lambda_5$	$147.35 + 19.52t$	$24.12 - 124.60t$
		16.1863 h	$\lambda_{514} + \lambda_5$	$77.02 - 288.66t$	$-205.62 - 55.10t$

Table 5. Rotational angles of the inner satellites of Jupiter (α_0, δ_0, W) and their secular, periodic, and mixed terms of the geodetic rotation

Metis (J16)	$\alpha_0 = 268.05 - 0.009T$ $\Delta\alpha_0 = 0.1241T - 0.00007T^2$ $- 8.590 \times 10^{-10} \cos(\text{J15}) + 1.424 \times 10^{-9} \sin(\text{J15})$ $- 2.068 \times 10^{-11}\, T\cos(\text{J15}) - 1.413 \times 10^{-11}\, T\sin(\text{J15})$ $- 7.330 \times 10^{-10} \cos(\text{J16}) - 3.720 \times 10^{-10} \sin(\text{J16})$ $+ 8.023 \times 10^{-12}\, T\cos(\text{J16}) - 1.750 \times 10^{-11}\, T\sin(\text{J16})$
	$\delta_0 = 64.49 + 0.003T$ $\Delta\delta_0 = - 0.0199T - 0.00004\, T^2$ $+ 2.620 \times 10^{-10} \cos(\text{J15}) + 1.306 \times 10^{-10} \sin(\text{J15})$ $- 1.233 \times 10^{-12}\, T\cos(\text{J15}) + 3.193 \times 10^{-12}\, T\sin(\text{J15})$ $+ 1.600 \times 10^{-10} \cos(\text{J16}) - 3.161 \times 10^{-10} \sin(\text{J16})$ $+ 7.374 \times 10^{-12}\, T\cos(\text{J16}) + 3.613 \times 10^{-12}\, T\sin(\text{J16})$
	$W = 33.29 + 1206.9986602\, d$ $\Delta W = - 0.0000232\, d + 4\times10^{-14}\, d^2$ $+ 1.076 \times 10^{-8} \cos(\text{J15}) - 9.604 \times 10^{-9} \sin(\text{J15})$ $+ 1.500 \times 10^{-10}\, T\cos(\text{J15}) + 1.671 \times 10^{-10}\, T\sin(\text{J15})$ $+ 6.420 \times 10^{-10} \cos(\text{J16}) + 3.344 \times 10^{-10} \sin(\text{J16})$ $- 6.380 \times 10^{-12}\, T\cos(\text{J16}) + 1.782 \times 10^{-11} T\sin(\text{J16})$
Adrastea (J15)	$\alpha_0 = 268.05 - 0.009T$ $\Delta\alpha_0 = 0.1217T - 0.00006T^2$ $+ 4.885 \times 10^{-10} \cos(\text{J13}) + 1.559 \times 10^{-9} \sin(\text{J13})$ $+ 2.235 \times 10^{-10} T\cos(\text{J13}) - 7.292 \times 10^{-11} T\sin(\text{J13})$ $- 7.523 \times 10^{-10} \cos(\text{J14}) + 2.984 \times 10^{-10} \sin(\text{J14})$ $+ 3.962 \times 10^{-11} T\cos(\text{J14}) + 1.021 \times 10^{-10} T\sin(\text{J14})$
	$\delta_0 = 64.49 + 0.003\, T$ $\Delta\delta_0 = -0.0195\, T - 0.00004\, T^2$ $+ 2.665 \times 10^{-10} \cos(\text{J13}) - 1.079 \times 10^{-10} \sin(\text{J13})$ $- 1.513 \times 10^{-11}\, T\cos(\text{J13}) - 3.958 \times 10^{-11} T\sin(\text{J13})$ $- 1.288 \times 10^{-10} \cos(\text{J14}) - 3.242 \times 10^{-10} \sin(\text{J14})$ $- 4.402 \times 10^{-11}\, T\cos(\text{J14}) + 1.734 \times 10^{-11} T\sin(\text{J14})$
	$W = 33.29 + 1206.9986602\, d$ $\Delta W = -0.0000227\, d + 4\times10^{-14}\, d^2$ $- 6.374 \times 10^{-11} \cos(\text{J13}) - 1.418 \times 10^{-8} \sin(\text{J13})$ $- 2.032 \times 10^{-9} T\cos(\text{J13}) + 1.056 \times 10^{-11} T\sin(\text{J13})$ $+ 6.654 \times 10^{-10} \cos(\text{J14}) - 2.579 \times 10^{-10} \sin(\text{J14})$ $- 3.175 \times 10^{-11} T\cos(\text{J14}) - 8.922 \times 10^{-11} T\sin(\text{J14})$

Table 5. (Contd.)

Amalthea (J5)	$\alpha_0 = 268.05 - 0.009T - 0.84\sin(\text{J1}) + 0.01\sin(2\,\text{J1})$ $\Delta\alpha_0 = 0.0518T - 0.00003T^2$ $- 1.091 \times 10^{-8}\cos(\text{J1}) + 4.759 \times 10^{-7}\sin(\text{J1})$ $+ 5.759 \times 10^{-8}\,T\cos(\text{J1}) - 1.618 \times 10^{-8}T\sin(\text{J1})$ $+ 1.424 \times 10^{-10}\cos(2\text{J1}) - 2.774 \times 10^{-9}\sin(2\text{J1})$ $- 3.866 \times 10^{-10}\,T\cos(2\text{J1}) + 1.040 \times 10^{-10}T\sin(2\text{J1})$ $- 7.333 \times 10^{-10}\cos(\text{J9}) - 1.016 \times 10^{-9}\sin(\text{J9})$ $- 1.531 \times 10^{-10}\,T\cos(\text{J9}) + 1.611 \times 10^{-10}T\sin(\text{J9})$ $+ 4.740 \times 10^{-10}\cos(\text{J10}) - 4.033 \times 10^{-10}\sin(\text{J10})$ $- 8.403 \times 10^{-11}\,T\cos(\text{J10}) - 6.913 \times 10^{-11}T\sin(\text{J10})$
	$\delta_0 = 64.49 + 0.003T - 0.36\cos(\text{J1})$ $\Delta\delta_0 = -0.0083T - 0.00002T^2$ $+2.057 \times 10^{-7}\cos(\text{J1}) - 1.972 \times 10^{-9}\sin(\text{J1})$ $- 6.964 \times 10^{-9}\,T\cos(\text{J1}) - 2.489 \times 10^{-8}T\sin(\text{J1})$ $- 9.629 \times 10^{-10}\cos(2\text{J1}) - 1.405 \times 10^{-11}\sin(2\text{J1})$ $+ 2.196 \times 10^{-11}\,T\cos(2\text{J1}) + 8.530 \times 10^{-11}T\sin(2\text{J1})$ $- 1.656 \times 10^{-10}\cos(\text{J9}) + 1.449 \times 10^{-10}\sin(\text{J9})$ $+ 3.135 \times 10^{-11}\,T\cos(\text{J9}) + 2.542 \times 10^{-11}T\sin(\text{J9})$ $+ 1.739 \times 10^{-10}\cos(\text{J10}) + 2.039 \times 10^{-10}\sin(\text{J10})$ $+ 2.980 \times 10^{-11}\,T\cos(\text{J10}) - 3.628 \times 10^{-11}T\sin(\text{J10})$
	$\text{W} = 231.67 + 722.6314560d + 0.76\sin(\text{J1}) - 0.01\sin(2\,\text{J1})$ $\Delta\text{W} = -0.0000097d + 2 \times 10^{-14}\,d^2$ $+ 3.907 \times 10^{-9}\cos(\text{J1}) - 4.044 \times 10^{-7}\sin(\text{J1})$ $- 5.001 \times 10^{-8}\,T\cos(\text{J1}) + 1.474 \times 10^{-8}T\sin(\text{J1})$ $- 1.267 \times 10^{-10}\cos(2\text{J1}) + 2.853 \times 10^{-9}\sin(2\text{J1})$ $+ 3.878 \times 10^{-10}T\cos(2\text{J1}) - 1.050 \times 10^{-10}T\sin(2\text{J1})$ $+ 3.527 \times 10^{-9}\cos(\text{J9}) + 1.030 \times 10^{-8}\sin(\text{J9})$ $+ 1.687 \times 10^{-9}T\cos(\text{J9}) - 9.374 \times 10^{-10}T\sin(\text{J9})$ $- 4.263 \times 10^{-10}\cos(\text{J10}) + 3.506 \times 10^{-10}\sin(\text{J10})$ $+ 7.343 \times 10^{-11}T\cos(\text{J10}) + 6.139 \times 10^{-11}T\sin(\text{J10})$
Thebe (J14)	$\alpha_0 = 268.05 - 0.009\,T - 2.11\sin(\text{J2}) + 0.04\sin(2\text{J2})$ $\Delta\alpha_0 = 0.0312\,T - 0.00002\,T^2$ $- 1.284\times10^{-7}\cos(\text{J2}) + 1.691 \times 10^{-6}\sin(\text{J2})$ $+ 3.038\times10^{-7}\,T\cos(\text{J2}) + 2.561 \times 10^{-8}\,T\sin(\text{J2})$ $+ 2.417\times10^{-9}\cos(2\text{J2}) - 2.937 \times 10^{-8}\sin(2\text{J2})$ $- 5.145\times10^{-9}\,T\cos(2\text{J2}) - 4.619 \times 10^{-10}\,T\sin(2\text{J2})$ $- 1.736\times10^{-10}\cos(\text{J11}) + 1.244 \times 10^{-9}\sin(\text{J11})$ $- 1.025\times10^{-10}\,T\cos(\text{J11}) - 1.443 \times 10^{-11}\,T\sin(\text{J11})$ $- 6.169\times10^{-10}\cos(\text{J12}) - 3.647 \times 10^{-11}\sin(\text{J12})$ $+ 4.938\times10^{-12}\,T\cos(\text{J12}) - 5.795 \times 10^{-11}\,T\sin(\text{J12})$

Table 5. (Contd.)

	$\delta_0 = 64.49 + 0.003T - 0.91\cos(J2) + 0.01\cos(2J2)$ $\Delta\delta_0 = -0.0050T - 0.00002\ T^2$ $+ 7.282 \times 10^{-7}\cos(J2) + 3.502 \times 10^{-8}\sin(J2)$ $+ 1.115 \times 10^{-8}\ T\cos(J2) - 1.311 \times 10^{-7}T\sin(J2)$ $-6.510 \times 10^{-9}\cos(2J2) - 4.351 \times 10^{-10}\sin(2J2)$ $- 1.171 \times 10^{-10}T\cos(2J2) + 1.131 \times 10^{-9}T\sin(2J2)$ $+ 2.223 \times 10^{-10}\cos(J11) + 1.410 \times 10^{-11}\sin(J11)$ $- 7.947 \times 10^{-13}T\cos(J11) + 1.754 \times 10^{-11}T\sin(J11)$ $+ 1.612 \times 10^{-11}\cos(J12) - 2.664 \times 10^{-10}\sin(J12)$ $+ 2.429 \times 10^{-11}T\cos(J12) + 1.468 \times 10^{-12}T\sin(J12)$
	$W = 8.56 + 533.7004100d + 1.91\sin(J2) - 0.04\sin(2J2)$ $\Delta W = -0.0000058d + 1 \times 10^{-14}\ d^2$ $+ 9.219 \times 10^{-8}\cos(J2) - 1.443 \times 10^{-6}\sin(J2)$ $- 2.651 \times 10^{-7}T\cos(J2) - 1.892 \times 10^{-8}T\sin(J2)$ $- 2.387 \times 10^{-9}\cos(2J2) + 2.933 \times 10^{-8}\sin(2J2)$ $+ 5.164 \times 10^{-9}T\cos(2J2) + 4.613 \times 10^{-10}T\sin(2J2)$ $+ 4.639 \times 10^{-9}\cos(J11) - 9.887 \times 10^{-9}\sin(J11)$ $+ 8.151 \times 10^{-10}T\cos(J11) + 3.821 \times 10^{-10}T\sin(J11)$ $+ 5.425 \times 10^{-10}\cos(J12) + 3.867 \times 10^{-11}\sin(J12)$ $- 3.672 \times 10^{-12}T\cos(J12) + 5.247 \times 10^{-11}T\sin(J12)$

T is the Barycentric Dynamical Time (BDT) measured in Julian centuries (36525 days) from the J2000 epoch;
d is the Barycentric Dynamical Time (BDT) measured in Julian days (jd) from the J2000 epoch; all angles (α_0, $\Delta\alpha_0$, δ_0, $\Delta\delta_0$, W, ΔW) are given in degrees;

$J1 = \Omega_{L55} = 73^\circ.32 + 91472^\circ.9T$,

$J2 = \Omega_{L514} = 24^\circ.62 + 45137^\circ.2T$, $J9 = \lambda_{55} - \lambda_5$, $J10 = \lambda_{55} + \lambda_5$, $J11 = \lambda_{514} - \lambda_5$,

$J12 = \lambda_{514} + \lambda_5$, $J13 = \lambda_{515} - \lambda_5$, $J14 = \lambda_{515} + \lambda_5$, $J15 = \lambda_{516} - \lambda_5$, $J16 = \lambda_{516} + \lambda_5$,

$\lambda_5 = 34^\circ.35 + 3034^\circ.9T = 0.59954632934 + 52.96909650946T$, $\lambda_{55} = 722^\circ.6314560d$,

$\lambda_{514} = 533^\circ.7004100d$, $\lambda_{515} = 1206^\circ.9986602d$, $\lambda_{516} = 1221^\circ.2547301d$.

comparable to their precession in the Newtonian approximation (see Table 5).

CONCLUSIONS

In this article, the rotational dynamics of the inner satellites of Jupiter, i.e., Metis, Adrastea, Amalthea, and Thebe, were considered. The study of the attitude stability of the plane synchronous rotation showed that the theoretically expected (Peale, 1977, 1999; Goldreich and Peale, 1966) and observed (Smith et al., 1979a; Thomas et al., 1998) plane synchronous rotation of all inner Jovian satellites for the most probable values of their figure parameters is stable relative to tilting the axis of rotation. On the stability diagrams constructed for all theoretically possible values of parameters of the figures of the satellites, the considered satellites are far from the regions with unstable dynamics. Perturbations in the rotational dynamics of satellites caused, e.g., by collisions (which do not lead to a significant change in the satellite figure) or close rapprochements with other bodies will not lead to satellites leaving the synchronous spin-orbital resonance. The possible evolution of the Amalthea figure, due to its very elongated shape, also will not lead to its exit from the observed mode of plane synchronous rotation.

The study of relativistic rotation of the inner satellites of Jupiter made it possible to determine, for the first time in the Euler angles and in the angles of their rotation relative to the Earth's fixed equator of the J2000.0 epoch, the most significant secular, periodic, and mixed terms of their geodetic rotation. This study showed that the value of geodetic rotation can be significant not only for objects that rotate around supermassive central bodies (neutron stars) but also for bodies with a short distance to the less massive central body, such as close satellites of giant planets. The analytical values obtained for the geodetic rotation of the inner satellites of Jupiter can be used for the numerical study of their rotation in the relativistic approximation.

FUNDING

This work was supported by the Russian Foundation for Basic Research, project no. 19-02-00811.

REFERENCES

Abalakin, V.K., *Osnovy efemeridnoi astronomii* (Fundamentals of Ephemeris Astronomy), Moscow: Nauka, 1979.

Archinal, B.A., Acton, C.H., A'Hearn, M.F., et al., Report of the IAU Working Group on cartographic coordinates and rotational elements: 2015, *Celest. Mech. Dyn. Astron.,* 2018, vol. 130, no. 22, pp. 1–46.

Barnard, E.E., Discovery and observations of a fifth satellite to Jupiter, *Astron. J.,* 1892, vol. 12, no. 275, pp. 81–85.

Beletskii, V.V., *Dvizhenie iskusstvennogo sputnika otnositel'no tsentra mass* (Movement of an Artificial Satellite Relative to the Center of Mass), Moscow: Nauka, 1965.

Biscani, F. and Carloni, S., A first-order secular theory for the post-Newtonian two-body problem with spin – II. A complete solution for the angular coordinates in the restricted case, *Mon. Notic. R. Astron. Soc.,* 2015, vol. 446, pp. 3062–3077.

Brumberg, V.A. and Bretagnon, P., Kinematical relativistic corrections for Earth's rotation parameters, *Proc. of IAU Colloquium 180,* 2000, pp. 293–302.

De Sitter, W., On Einstein's theory of gravitation and its astronomical consequences, *Mon. Notic. R. Astron. Soc.,* 1916, no. 77, pp. 155–184.

Eroshkin, G.I. and Pashkevich, V.V., Geodetic rotation of the Solar system bodies, *Artif. Satell.,* 2007, vol. 42, no. 1, pp. 59–70.

Folkner, W.M., Williams, J.G., Boggs, D.H., Park, R.S., and Kuchynka, P., *The Planetary and Lunar Ephemerides DE430 and DE431, IPN Prog. Report 42–196,* 2014, pp. 1–81.

Fukushima, T., Geodesic nutation, *Astron. Astrophys.,* 1991, vol. 244, no. 1, pp. L11–L12.

Giorgini, J.D., Chodas, P.W., and Yeomans, D.K., Orbit uncertainty and close-approach analysis capabilities of the Horizons On-Line Ephemeris System, *33rd AAS/DPS Meeting in New Orleans,* Los Angeles, 2001.

Goldreich, P. and Peale, S., Spin-orbit coupling in the Solar system, *Astron. J.,* 1966, vol. 71, no. 6, pp. 425–438.

Kopeikin, S., Efroimsky, M., and Kaplan, G., *Relativistic Celestial Mechanics in the Solar System,* Hoboken, NY: John Wiley and Sons, 2011.

Kouprianov, V.V. and Shevchenko, I.I., On the chaotic rotation of planetary satellites: The Lyapunov exponents and the energy, *Astron. Astrophys.,* 2003, vol. 410, pp. 749–757.

Lichtenberg, A.J. and Lieberman, M.A., *Regular and Stochastic Motion,* Springer-Verlag New York, 1983.

Ma, C., Arias, E.F., Eubanks, T.M., et al., The international celestial reference frame as realized by very long baseline interferometry, *Astron. J.,* 1998, vol. 116, pp. 516–546.

Melnikov, A., Pashkevich, V., Vershkov, A., and Karelin, G., *Chaos and relativistic effects in the rotational dynamics of minor planetary satellites, Proc. Journées 2019 Astrometry, Earth Rotation and Reference Systems in the Gaia Era*, Ed. by Bizouard, C. (Observatoire de Paris, Paris, France, 07–09 October 2019), pp. 339–344 (Pub Date September 2020, Bibcode: 2020jsrs.conf.339M.)

Melnikov, A.V. and Shevchenko, I.I., On the rotational dynamics of Prometheus and Pandora, *Celest. Mech. Dynam. Astron.,* 2008, vol. 101, nos. 1–2, pp. 31–47.

Melnikov, A.V. and Shevchenko, I.I., On the stability of the rotational motion of nonspherical natural satellites in a synchronous resonance, *Sol. Syst. Res.,* 2000, vol. 34, no. 5, pp. 434–442.

Melnikov, A.V. and Shevchenko, I.I., Unusual rotation modes of minor planetary satellites, *Sol. Syst. Res.,* 2007, vol. 41, no. 6, pp. 483–491. https://doi.org/10.1134/S0038094607060032

Pashkevich, V.V. and Eroshkin, G.I., Relativistic rotation of the rigid body in the Rodrigues–Hamilton parameters: Lagrange function and equations of motion, *Artif. Satell.,* 2018, vol. 53, no. 3.

Pashkevich, V.V. and Vershkov, A.N., Consideration of relativistic effects in the rotation of Mars and its satellites, *Sol. Syst. Res.,* 2019, vol. 53, no. 6, pp. 431–435. https://doi.org/10.1134/S0038094619060066

Pashkevich, V.V. and Vershkov, A.N., New high-precision values of the geodetic rotation of the mars satellites system, major planets, Pluto, the Moon and the Sun, *Artif. Satell.,* 2019, vol. 54, no. 2, pp. 31–42.

Pashkevich, V.V., Geodesic (relativistic) rotation of bodies in the Solar system, *Vestn. S.-Peterb. Gos. Univ., Ser. 1,* 2016, vol. 3, no. 61, pp. 506–516.

Peale, S.J., Origin and evolution of the natural satellites, *Annu. Rev. Astron. Astrophys.,* 1999, vol. 37, pp. 533–602.

Peale, S.J., Rotation histories of the natural satellites, in *Planetary Satellites,* Burns, J.A., Eds., Tucson: Univ. Arizona Press, 1977, pp. 87–112.

Porco, C.C. and the Cassini Imaging Team, Cassini imaging of Jupiter's atmosphere, satellites and rings, *Science,* 2003, vol. 299, pp. 1541–1547.

Shevchenko, I.I., The separatrix algorithmic map: Application to the spin-orbit motion, *Celest. Mech. Dyn. Astron.,* 1999, vol. 73, pp. 259–268.

Smith, B.A. and the Voyager Imaging Team, Jupiter system through the eyes of Voyager-1, *Science,* 1979a, vol. 204, pp. 951–972.

Smith, B.A. and the Voyager Imaging Team, The Galilean satellites and Jupiter: Voyager-2 imaging results, *Science,* 1979b, vol. 206, pp. 927–950.

Thomas, P.C., Burns, J.A., Rossier, L., Simonelli, D., et al., The small inner satellites of Jupiter, *Icarus,* 1998, vol. 135, pp. 360–371.

Tiscareno, M.S., Thomas, P.C., and Burns, J.A., The rotation of Janus and Epimetheus, *Icarus,* 2009, vol. 204, pp. 254–261.

Torzhevskii, A.P., Periodic solutions of the equation of plane oscillations of a satellite in an elliptical orbit, *Kosmich. Issled.,* 1964, vol. 2, no. 5, pp. 667–678.

Wisdom, J., Rotation dynamics of irregularly shaped natural satellites, *Astron. J.,* 1987, vol. 94, no. 5, pp. 1350–1360.

Woolard, E.W., *Theory of the Rotation of the Earth around Its Center of Mass,* Univ. Calif. Libr., 1963.

Translated by O. Pismenov